# Scanning tunneling microscopy and spectroscopy studies of the surface structure and electronic properties of single-crystal Tl–Ba–Ca–Cu–O superconductors

Zhe Zhang and Charles M. Lieber
*Department of Chemistry, Columbia University, New York, NY 10027*

David S. Ginley, Robert J. Baughman, and Bruno Morosin
*Sandia National Laboratories, Albuquerque, New Mexico 87185*

(Received 24 July 1990; accepted for publication 8 November 1990)

Scanning tunneling microscopy (STM) and scanning tunneling spectroscopy (STS) have been used to characterize the surface structure and electronic properties of $Tl_2Ba_2CaCu_2O_8$ and $Tl_2Ba_2Ca_2Cu_3O_{10}$ single crystals. Atomic resolution STM images show that 90%–95% of the surface has a near-trigonal structure with $a = b = 0.24$ nm and an $a$–$b$ angle of 65°. The remaining 5%–10% of the surface consists of a new orthorhombic structure with $a = b = 0.40$ nm. Spatially resolved STS measurements further demonstrate that regions with the 0.24 nm period structure are metallic, while areas with the 0.40 nm period structure are semiconducting.

## I. INTRODUCTION

Extensive studies since the discovery of high-temperature superconductivity in the Tl–Ba–Ca–Cu–O system[1–6] have led to the development of two families of thallium containing materials that have the general structural formulas $Tl_2Ba_2Ca_{n-1}Cu_{2n+4}$ and $TlBa_2Ca_{n-1}Cu_nO_{2n+3}$.[6] The highest documented superconducting transition temperature ($T_c$) in these systems is 125 K for $Tl_2Ba_2Ca_2Cu_3O_{10}$.[4] The tetragonal crystal symmetry and average atomic positions of these materials have been well characterized using x-ray,[2–6] neutron,[7] and electron[8] diffraction. Other more subtle points such as thallium and oxygen positional disorder, oxygen vacancies, and cationic substitution remain to be defined. The local nature of these interesting structural features make them difficult to address using diffraction techniques, although it is believed that structural and compositional inhomogeneities may play an important role in determining the superconducting properties of the Tl-based materials. To address directly the thallium and oxygen bonding as well as other localized structural and electronic features in the Tl-based materials we have been using scanning tunneling microscopy (STM) and scanning tunneling spectroscopy (STS),[9] and herein we report recent studies of $Tl_2Ba_2CaCu_2O_8$ and $Tl_2Ba_2Ca_2Cu_3O_{10}$ single crystals.

## II. EXPERIMENTAL

The crystal growth procedure for the preparation of $Tl_2Ba_2CaCu_2O_8$ and $Tl_2Ba_2Ca_2Cu_3O_{10}$ crystals has been described previously.[6,10] Briefly, crystals were grown by a pseudo-flux method from melts of composition $Tl_4Ba_1Ca_3Cu_4$ and $Tl_4Ba_1Ca_3Cu_{10}$, respectively, made up of high-purity (>99.99%) oxides that were stored and processed in an argon atmosphere dry box. The mixtures, sealed in Pt crucibles with tight-fitting Pt lids, were rapidly heated in a vertical tube furnace under one atmosphere of oxygen to 950 °C. The crucible was maintained at 950 °C for 1 h, cooled to 700 °C over 12.5 h, and finally cooled to 25 °C in 5–6 h. The resulting plate-like crystals were analyzed using energy-dispersive x-ray analysis (EDS) and x-ray precession photography. EDS was performed on both crystal faces to identify crystals with $Tl_2Ba_2CaCu_2O_8$ and $Tl_2Ba_2Ca_2Cu_3O_{10}$ composition. X-ray diffraction analysis of these crystals showed only minor intergrowths.

The STM and STS studies were performed in an argon-filled glove box equipped with a purification system that reduced the concentrations of $H_2O$ and $O_2$ to below 1 ppm. Commercial and modified[11] STMs (Nanoscope, Digital Instruments, Inc., Santa Barbara, CA) were used to acquire the image data. The modified STM was also used for all of the spectroscopy studies. The STS current ($I$) versus voltage ($V$) data were acquired by interrupting the STM feedback loop, and then stepping the sample-tip bias voltage while digitally storing the resulting changes in tuneling current. The $I$-$V$ data shown are the average of 20 to 40 curves obtained at a selected surface site; these measurements represent an average over several atomic positions due to drifts during data acquisition. The STM and STS measurements were made on cleaved sample surfaces using platinum-iridium (80%-20%) alloy tips. The cleaved surfaces were oriented with the $c$- axis parallel to the tip.

## III. RESULTS AND DISCUSSION

Atomic resolution images of a cleaved $Tl_2Ba_2CaCu_2O_8$ crystal are shown in Fig. 1. These images are typical of the data observed over 90%–95% of the surface. Analysis of these images shows that the surface structure is near trigonal with $a = b = 0.24 \pm 0.02$ nm and an $a$–$b$ lattice angle of $65° \pm 5°$. Similar images of the $Tl_2Ba_2CaCu_2O_8$ surfaces were obtained using both positive and negative bias voltages from $-600$ to $+600$ mV; images of $Tl_2Ba_2Ca_2Cu_3O_{10}$ crystal surfaces also exhibited the same lattice features within experimental error. The 0.24 nm average peak separation observed in these images is similar to the average in-plane Tl–O separation reported in x-ray diffraction studies.[3] In contrast, the Cu–O separation, 0.193 nm, is significantly shorter, while the 0.277 nm Ba–O distance is longer.[3] The

 0734-211X/91/021009-04$01.00  

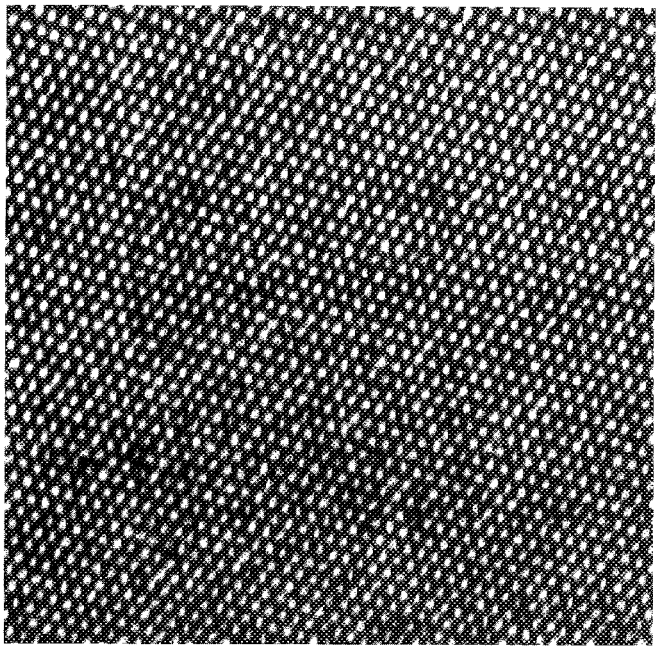

(a)

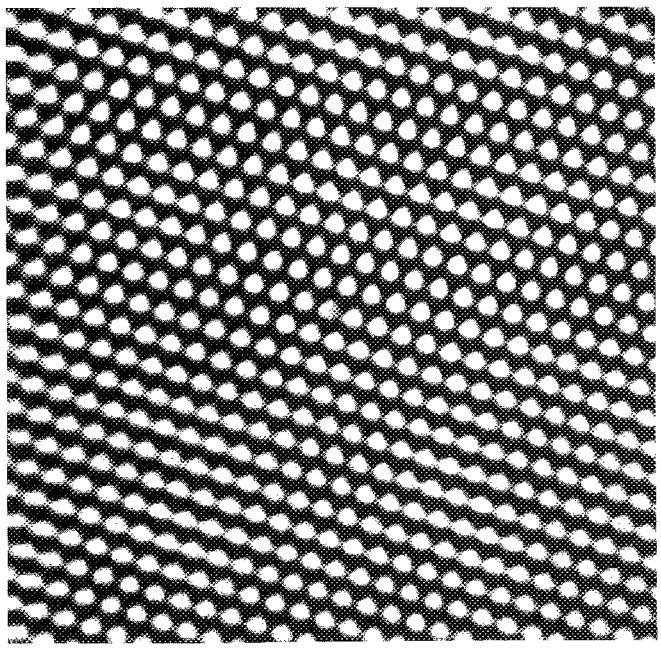

(b)

FIG. 1. (a) A $10\times10$ nm$^2$ grey scale image of a single-crystal $Tl_2Ba_2CaCu_2O_8$ sample recorded with a bias voltage of $-165$ mV and a tunneling current of 1.9 nA. The data is unfiltered. The structure in the image has near trigonal symmetry with $a=b=0.24\pm0.2$ nm. (b) A $6.0\times6.0$ nm$^2$ image recorded on a independent $Tl_2Ba_2CaCu_2O_8$ crystal with a bias voltage of $-165$ mV and a tunneling current of 1.9 nA. The near trigonal lattice ($a\approx b\approx0.24$ nm) is the same as in (a).

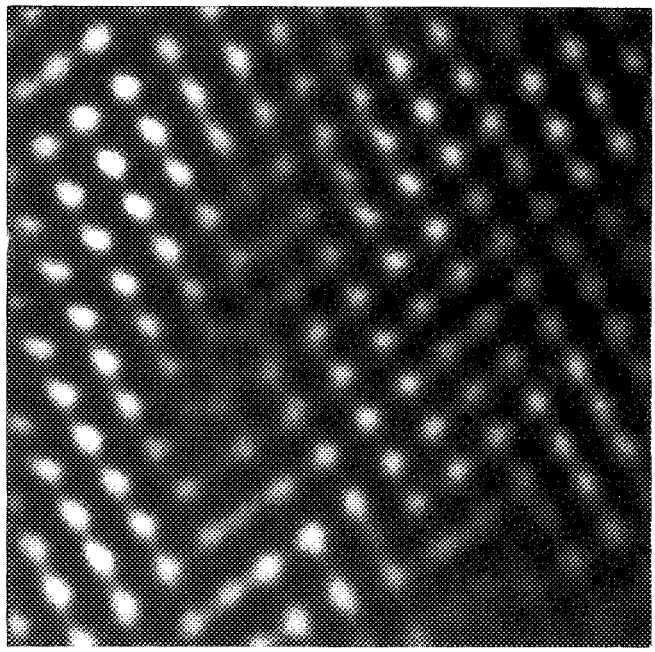

(c)

FIG. 2. A $6.0\times6.0$ nm$^2$ image of a $Tl_2Ba_2CaCu_2O_8$ sample recorded with a bias voltage of $-330$ mV and a tunneling current of 2.1 nA. The orthorhombic structure observed in this image has a period of 0.46 nm. This structure is observed over 5%–10% of the surface.

ionic Ba–O layer also does not contribute appreciably to the density of states near the Fermi level[12] (i.e., this layer does not contribute to the density of states probed in our STM experiments). We therefore assign the atomic structure observed in the STM images to the Tl and O sites.

The surface Tl–O structure shown in Fig. 1 is highly distorted from the average tetragonal crystal symmetry determined from diffraction investigations.[2-8] There are two likely explanations for the near trigonal (versus tetragonal) structure observed in the images. First, it is possible that the Tl–O layer structure is intrinsically distorted throughout the bulk of the crystal. In support of this possibility we note that x-ray[3] and neutron[7] diffraction data suggest that the Tl and O atoms do not occupy ideal tetragonal crystal sites. Since a good refinement of the Tl and O positions has not yet been reported we cannot, however, unambiguously correlate the distorted surface structure with bulk Tl and O disorder. Alternatively, the near trigonal structure observed in our images could be due to a surface reconstruction; that is, since relatively short out of plane Tl–O bonds are broken when the crystals are cleaved it is possible that the resulting Tl–O surface will relax.

Irrespective of the exact origin of the near trigonal surface structure, the observation of both atomic sites in images such as Fig. 1 demonstrate that Tl and O make comparable contributions to the density of states near the Fermi level. We thus conclude that the distorted surface structure does not adversely affect the formation of covalent Tl–O bonds and a delocalized metallic band. Electronic structure calculations indicate for an undistorted tetragonal structure that Tl and O will contribute unequally to the density of states at the Fermi level[12] in contrast to our experimental images. More recent calculations carried out for a distorted Tl–O structure show, however, that distorted Tl–O bonding yields a metallic band.[13] Notably, STM images of the Bi-O layer in the structurally related material $Bi_2Sr_2CaCu_2O_8$ exhibit tetragonal structure with semiconducting electronic proper-

ties.[14] It is thus interesting to speculate whether distortions of the Tl-O layer that yield a metallic band could explain the large difference in $T_c$ for the structurally similar Tl- and Bi-based materials.

In addition to the 0.24-nm-period structure discussed above, we have characterized a new structure that has a period of 0.40 nm (Fig. 2). This orthorhombic structure is observed over 5%–10% of the surface. The localized and random appearance of this new structure suggests that it is probably due to compositional inhomogeneities in the Tl–O layer. Analysis of images containing both the 0.24 and 0.40 nm structural regions provide further insight into the nature of this new structure (Fig. 3). In the large-area image [Fig. 3(a)] both the 0.24- and 0.40-nm-period structures are shown. The angle between these two lattices is 150°. A high-resolution image of the region between the two structures demonstrates that they are not separated by an abrupt boundary or crystal defect [Fig. 3(b)]. Specifically, there is a gradual decrease in the tunneling contribution from atomic sites across the boundary. These data indicate that the electronic structure probably becomes more localized (less metallic) in the 0.40 nm period regions. The 0.40 nm structure may be attributed to the observation of alternate atomic positions as in images of the Bi–O layer of $Bi_2Sr_2CaCu_2O_8$[14] since the average Tl–Tl or O–O separation is only 0.38 nm.

To characterize better the electronic structure of these two distinct regions we have made spatially resolved STS measurements. Typical $I$–$V$ data recorded over the 0.24 and 0.46 nm structures are shown in Fig. 4. In addition, the normalized conductivity, $(V/I)dI/dV$, for these two data sets are plotted in this figure since $(V/I)dI/dV$ is proportional to the local density of states at the sample surface. These data (e.g., Fig. 4) show that there are significant differences in the electronic structure of the 0.24 and 0.40 nm regions. For areas exhibiting the 0.24 nm structure the density of states increases continuously above and below the Fermi level; these data are indicative of a metallic surface. In contrast, for regions exhibiting the 0.40 nm structure there is an apparent gap (100–200 mV) in the density of states at the Fermi level. Similar STS results have also been obtained over areas of $Tl_2Ba_2Ca_2Cu_3O_{10}$ crystals that show the 0.24 and the 0.40 nm structure. The gap in the density of electronic states observed in the STS data recorded over the regions exhibiting 0.40 nm structure supports our proposal that this structure is due to compositional inhomogeneities in the Tl–O layer since substitution of $Ca^{2+}$ for $Tl^{3+}$ in the Tl–O layer or oxygen vacancies would cause localization of the electronic states.

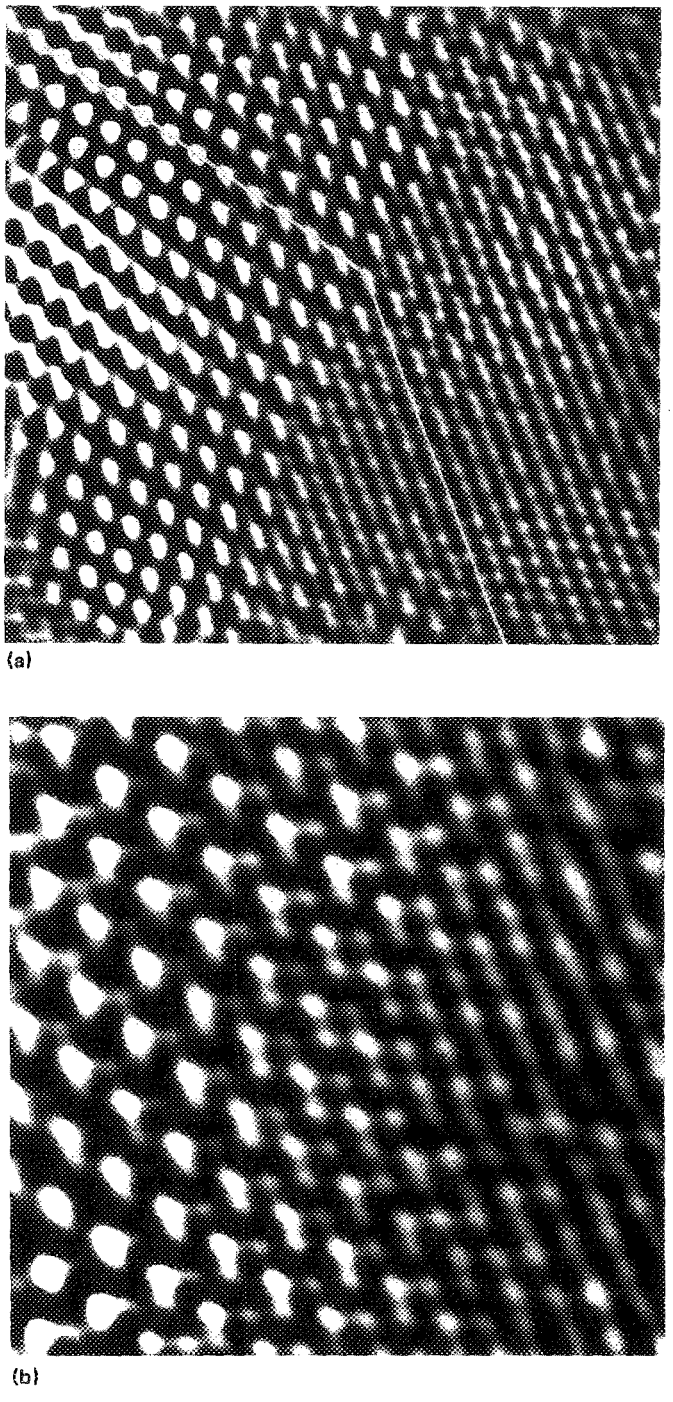


FIG. 3. (a) A $8.0\times8.0$ nm$^2$ image recorded with a bias voltage of $-100$ mV and a tunneling current of 1.2 nA. The atomic structure observed on the right side of the image has a period of 0.24 nm, while the structure observed on the left side has a period of 0.40 nm. The angle between these two structures is highlighted by lines in (a). (b) A high-resolution ($4.0\times4.0$ nm$^2$) image of the boundary between the surface regions that exhibit 0.24- and 0.46-nm-period structure.

## IV. CONCLUSIONS

In summary, we have used STM and STS to characterize the surface structure and electronic properties of the Tl–O layer in $Tl_2Ba_2CaCu_2O_8$ and $Tl_2Ba_2Ca_2Cu_3O_{10}$ single crystals. Atomic resolution images show that 90%–95% of the surface structure is near trigonal with $a = b = 0.24$ nm; this structure corresponds to the Tl and O sites. The remaining 5–10% of the surface, however, consists of an orthorhombic lattice with $a = b = 0.40$ nm. Spatially resolved STS measurements have further shown that the 0.24 nm period regions are metallic, while the 0.40 nm period areas are semiconducting. These STM and STS data are consistent with inhomogeneous cationic substitution and/or oxygen vacancies in the Tl–O layer that cause electronic localization. In the future it will be important to determine how

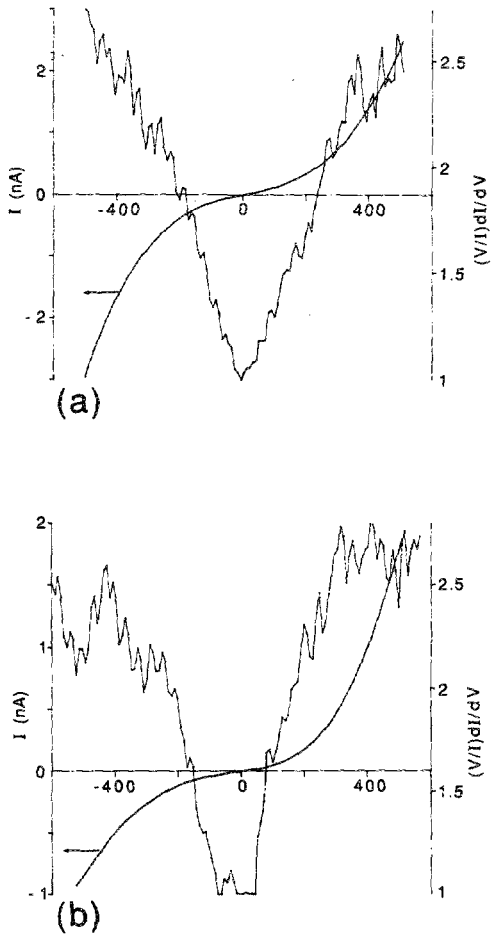


FIG. 4. Typical current-voltage and $(V/I)dI/dV$ curves for (a) a 0.24 nm structural region and (b) a 0.40 nm structural region. The normalized conductivity curves, $(V/I)dI/dV$, were obtained by numerically differentiating the current-voltage data. The $x$ axis in (a) and (b) is in millivolts.

these electronically distinct regions affect the superconducting properties in the $Tl_2Ba_2Ca_{n-1}Cu_nO_{2n+4}$ materials.

## ACKNOWLEDGMENTS

C. M. L. acknowledges support of the work at Columbia University by the National Science Foundation and the David and Lucile Packard Foundation. The work at Sandia National Laboratories was supported, in part, by the United States Department of Energy, Office of Basic Energy Sciences, under Contract No. DE-AC04-76DP00789. The technical assistance of M. A. Mitchell is gratefully acknowledged.

[1] Z. Z. Sheng and A. M. Hermann, Nature **332**, 138 (1988).
[2] R. M. Hazen, L. W. Finger, R. J. Angel, C. T. Prewitt, N. L. Ross, C. G. Hadidiacos, P. J. Heaney, D. R. Veblen, Z. Z. Sheng, A. El Ali, and A. M. Hermann, Phys. Rev. Lett. **60**, 1657 (1988).
[3] C. C. Torardi, M. A. Subramanian, J. C. Calabrese, J. Gopalakrishnan, K. J. Morrissey, T. R. Askew, R. B. Flippen, U. Chowdhry, and A. W. Sleight, Science **240**, 631 (1988).
[4] S. S. P. Parkin, V. Y. Lee, E. M. Engler, A. I. Nazzal, T. C. Huang, G. Gorman, R. Savoy, and R. Beyers, Phys. Rev. Lett. **60**, 2539 (1988).
[5] B. Morosin, D. S. Ginley, E. L. Venturini, P. F. Hlava, R. J. Baughman, J. F. Kwak, and J. E. Schirber, Physica C **152**, 223 (1988).
[6] B. Morosin, R. J. Baughman, D. S. Ginley, J. E. Schirber, and E. L. Venturini, Physica C **161**, 115 (1990).
[7] D. E. Cox, C. C. Torardi, M. A. Subramanian, J. Gopalakrishnan, and A. W. Sleight, Phys. Rev. B **38**, 6624 (1988).
[8] R. Beyers, S. S. P. Parkin, V. Y. Lee, A. I. Nazzal, R. Savoy, G. Gorman, and S. La Placa, Appl. Phys. Lett. **53**, 432 (1988).
[9] X. L. Wu, C. M. Lieber, D. S. Ginley, and R. J. Baughman, Appl. Phys. Lett. **55**, 2129 (1989).
[10] D. S. Ginley, B. Morosin, R. J. Baughman, E. L. Venturini, J. E. Schirber, and J. F. Kwak, J. Cryst. Growth **91**, 456 (1988).
[11] Z. Zhang and C. M. Lieber (to be published).
[12] J. Yu, S. Massidda, and A. J. Freeman, Physica C **152**, 273 (1988).
[13] D. Jung, M.-H. Whangbo, N. Herron, and C. C. Torardi, Physica C **160**, 381 (1989).
[14] X. L. Wu, Z. Zhang, Y. L. Wang, and C. M. Lieber, Science **248**, 1211 (1990).